Hindawi Publishing Corporation
Journal of Nanomaterials
Volume 2015, Article ID 416012, 10 pages
http://dx.doi.org/10.1155/2015/416012

Research Article

Functionalized Magnetic Nanoparticles and Their Effect on *Escherichia coli* and *Staphylococcus aureus*

Mohamed S. A. Darwish,[1,2] Nhung H. A. Nguyen,[1] Alena Ševců,[1] and Ivan Stibor[1]

[1] *Institute for Nanomaterials, Advanced Technologies and Innovation, Technical University of Liberec, Studentská 2, 461 17 Liberec, Czech Republic*
[2] *Egyptian Petroleum Research Institute, 1 Ahmed El-Zomor Street, El Zohour Region, Nasr city, Cairo 11727, Egypt*

Correspondence should be addressed to Mohamed S. A. Darwish; msa.darwish@gmail.com and Ivan Stibor; ivan.stibor@tul.cz

Received 8 December 2014; Accepted 1 March 2015

Academic Editor: Piaoping Yang

Magnetite (Fe_3O_4) nanoparticles were prepared using coprecipitation and subsequently surface-functionalized with 3-aminopropyltriethoxysilane (APTS), polyethylene glycol (PEG), and tetraethoxysilane (TEOS). Nanoparticle morphology was characterized using scanning electron microscopy, while structure and stability were assessed through infrared spectroscopy and zeta potential, respectively. Average size of the nanoparticles analysed by dynamic light scattering was 89 nm, 123 nm, 109 nm, and 130 nm for unmodified magnetite and APTS-, PEG-, and TEOS-modified magnetite nanoparticles, respectively. Biological effect was studied on two bacterial strains: Gram-negative *Escherichia coli* CCM 3954 and Gram-positive *Staphylococcus aureus* CCM 3953. Most of modified magnetite nanoparticles had a significant effect on *S. aureus* and not on *E. coli*, whereas PEG-magnetite nanoparticles displayed no significant effect on the growth rate of either bacteria.

1. Introduction

Surface functionalized magnetic nanoparticles have been widely used in a range of biological applications [1–3]. Magnetite (Fe_3O_4) is easily degradable and is useful, therefore, in bioseparation and catalytic processes. Magnetite nanoparticles have also been extensively studied in biomedicine [4, 5] due to their superparamagnetic properties, high biocompatibility, and lack of toxicity to humans. Magnetite nanoparticles possess high surface energy and thus tend to quickly aggregate. Such strong aggregation, however, may alter their adsorption properties and magnetic efficiency; hence the nanoparticles are frequently coated with an organic or inorganic layer to prevent aggregation. Such coatings not only stabilize the magnetite nanoparticles but can be easily used for further functionalization. Uncoated magnetite nanoparticles are also known to be highly susceptible to leaching under acidic conditions; hence several methods have been developed for the preparation of magnetic nanoparticles coated with a polymer, such as polyethylene glycol (PEG) and silica-containing organic material [6–8] in the form of a core/shell structure, with the silica/PEG shell coated onto magnetic nanoparticles [9, 10]. Described coating enhances hydrophilicity and improves biocompatibility [11, 12]; the core/shell structure [13] has a number of attractive properties, including high adsorption capacity and chemical and thermal stability [14]. As the shell provides active groups on its surface that make available binding sites for enzymes, proteins, or drugs [15], magnetic nanoparticles have the potential to serve as drug carriers that can selectively target cancer cells, for example, and provide controlled release of chemotherapeutics [16, 17]. Magnetite nanoparticles coated with aminopropyltriethoxysilane (APTS) have many applications as adsorbent layers for removal of aqueous heavy metals during waste water treatment [18, 19]. Finally, the nontoxic nature of PEG-modified nanoparticles may be useful for more efficient biotechnology application [20].

Coprecipitation, sol-gel, and microemulsion are some of the most common methods for superparamagnetic magnetite nanoparticle synthesis, with coprecipitation being the most simple and economic method [21, 22]. It is based on the mixing of probably Fe^{3+} and Fe^{2+} at a 2 : 1 molar ratio in a highly basic solution, with the size and shape of the magnetite nanoparticles produced depending on the type of salt used,

the reaction temperature, pH, and ionic strength of the media. A common method for coating magnetite nanoparticles with a uniform silica shell is the sol-gel process. This process makes use of base-catalyzed hydrolysis and condensation of tetraethoxysilane (TEOS) [23]. The shell thickness of these silica-coated magnetite nanoparticles can be adjusted by controlling the amount of TEOS used [24].

The use of nanoscale materials has also attracted increasing concern due to the potential for environmental risk of toxicity. Several studies have been performed to evaluate the toxicity of magnetite nanoparticles on eukaryotic organisms, with surfactant-modified magnetite nanoparticles displaying negligible toxicity [25, 26]. Few studies have been published on the toxicity of magnetite nanoparticles to bacteria [27–33]; hence it is important to study the toxic effects of modified magnetite nanoparticles on more bacterial strains in order to fill gaps in our knowledge.

In this study, we prepared a range of magnetite nanoparticles with different surface functionality by modifying the nanoparticle surface with either APTS, PEG, or TEOS. The functional groups, surface charge, diameter, and morphology of the nanoparticles were characterized, together with their biological effect on Gram-negative *Escherichia coli* and Gram-positive *Staphylococcus aureus*.

2. Materials and Methods

2.1. Chemicals and Characterization. Iron (III) chloride hexahydrate ($FeCl_3{\cdot}6H_2O$, ≥98%), iron (II) chloride tetrahydrate ($FeCl_2{\cdot}4H_2O$, ≥99%), ammonium hydroxide (26% NH_3 in H_2O), PEG (PEG6000, ≥95%), APTS (≥97%), and TEOS (≥99%) were purchased from Sigma-Aldrich and used as received. Nanoparticle structure and stability were assessed through infrared spectroscopy and zeta potential, respectively. Fourier transform infrared spectroscopy (FT-IR) was performed using the Tensor 27 Infrared Spectrometer (Bruker, USA), while zeta potential measurements were performed using a Zetasizer Nano analyzer (Malvern Instruments, USA) at pH 7. Dynamic light scattering (DLS) analysis was employed to measure the hydrodynamic diameters of magnetic nanoparticle aggregates in DI water using a Zetasizer Nano DLS unit. Microscopy images were obtained through scanning electron microscopy (SEM) using a Zeiss ULTRA Plus field-emission SEM equipped with a Schottky cathode. The images were analyzed using Smart SEM software v5.05 (Zeiss, Germany) for imaging operated at 1.5 kV.

2.2. Synthesis of Unmodified Magnetite Nanoparticles. The unmodified magnetite nanoparticles were produced from an aqueous solution of $FeCl_3{\cdot}6H_2O$ and $FeCl_2{\cdot}4H_2O$ using the coprecipitation method [21, 22]. $FeCl_2{\cdot}4H_2O$ (1.9 g) and $FeCl_3{\cdot}6H_2O$ (5.4 g) at an Fe^{3+}/Fe^{2+} molar ratio of 2 : 1 were dissolved in deionized water (DI; 100 mL) and heated to 70°C. Ammonium hydroxide (6 mL) was quickly added to the solution, which immediately produced a deep black magnetite precipitate. The suspension was stirred for 30 min at 70°C. The product was washed several times with distilled water, following which the magnetite nanoparticles were dried in a rotary evaporator at 40°C (25 mbar) until a powder was formed. The powdered nanomaterial was stored in the dark at room temperature prior to modification.

APTS-modified magnetite nanoparticles were prepared according to Ming et al. [34, 35], with minor modification. A 0.0128 M of magnetite solution (25 mL), which was prepared from first experiment, was diluted to 150 mL with ethanol (absolute) and 1 mL DI water. This solution was then treated in an ultrasonic bath (28 kHz at 25°C) for 1 h, whereupon APTS (35 μL) was added and stirred rapidly for 2 h. The resulting liquid was washed with ethanol five times and then dried in a vacuum at room temperature until a powder was formed.

PEG-modified magnetite nanoparticles were prepared by dissolving 1.99 g of $FeCl_2{\cdot}4H_2O$ and 3.24 g of $FeCl_3{\cdot}6H_2O$ in 50 mL of DI water (Beaker I) and 30 mL of ammonium hydroxide in 50 mL of DI water (Beaker II). Subsequently, 2.5 g of PEG 6000 was dissolved in 100 mL of DI water and the liquid stirred at room temperature. The PEG solution (25 mL) was added to both beakers (I and II) and stirred in order to obtain a homogenous solution. The contents of Beaker II were added dropwise to Beaker I until pH 9 was reached. Formation of the magnetic nanoparticles was confirmed through a color change in the solution [36, 37]. The nanoparticles were separated out by centrifuging (28 kHz for 30 minutes) and the resultant precipitate was dried for 24 hours at room temperature. The dried powder was then redissolved in the remaining 50 mL of PEG solution and placed in an ultrasonic bath for about 30 minutes, whereupon it was again centrifuged to obtain the magnetic PEG-nanoparticles, which were then washed several times with DI water and dried to a powder under vacuum at room temperature.

TEOS-modified magnetite nanoparticles were prepared by dispersing approximately 30 mg of freshly prepared magnetite nanoparticles in 30 mL of ethanol and 6 mL of DI water, with the dispersion then being homogenized in an ultrasonic bath (28 kHz at 25°C) for about 10 minutes. TEOS (3.3 mmol) was then added to the mixture and sonicated for a further 20 minutes. Finally, aqueous ammonia (30 mmol) was added and the mixture again was placed in an ultrasonic bath for 60 minutes. The magnetic nanoparticles were magnetically separated and washed several times with DI water and then dried to a powder under vacuum at room temperature [38–41].

2.3. Dispersion of Magnetite Nanoparticles. To assess the effect of functionalized magnetite nanoparticles on bacteria, stock solutions (10 g/L) of unmodified magnetite and APTS-, PEG-, TEOS-modified magnetite nanoparticles were prepared from powdered material (see above) by dispersing in sterilized DI water in a sterile glass tube and vortexing (IKA vortex3, Germany) for five minutes. Each suspension was prepared freshly before testing for toxicity.

2.4. Bacterial Strains and Culture Media. Bacterial strains of Gram-negative *E. coli* CCM 3954 and Gram-positive *S. aureus* CCM 3953 were obtained from the Czech Collection of

Microorganisms, Masaryk University, Brno, Czech Republic. The bacterial inocula were always prepared freshly from a single colony growing overnight in a soya nutrient broth (Sigma Aldrich) at 37°C. The culture was adjusted to 0.01–0.02 optical density (OD) at 600 nm (OD_{600}) using the DR6000 UV-Vis spectrophotometer (Hach Lange, Germany), immediately before performing the antibacterial experiments.

2.5. Bacterial Growth Rate. The freshly prepared bacterial cultures were transferred to 30 mL of soya broth and kept in 200 mL conical flasks. The magnetite suspensions (unmodified and APTS-, PEG-, TEOS-modified) were added to the bacterial culture at a range of final concentrations (0.05, 0.3, 0.6, and 1 g/L), each sample being prepared in replicate. Negative (bacterial cells only in growth media) and positive (magnetic nanoparticles only in growth media) controls were run in parallel. All samples were incubated for six hours at 37°C. Subsamples were taken every two hours for OD_{600} measurement. To prevent cross contamination, each bacterial strain was tested on different days. Oxidative/reductive potential (ORP) and pH were measured during the experiments using a WTW multimeter (Germany).

Effect of nanoparticle concentration on bacterial growth rate (μ) was calculated for each nanoparticle type based on the equation: $I(\%) = (\mu_C - \mu_T)/\mu_C \times 100$, where I is inhibition, μ_C is mean value of growth rate (μ) of the control, and μ_T value is the growth rate of the culture affected by the nanoparticles. The bacterial growth rate was defined by R linear regression of cell density (OD_{600}) versus incubation time (hour). The EC10 value (effective concentration at 10% inhibition) was obtained by plotting I% versus concentration of nanoparticle tested.

2.6. Determination of Colony Forming Units (CFU). Number of *E. coli* and *S. aureus* CFU was determined using the same unmodified and APTS-, PEG-, and TEOS-modified magnetite (1 g/L) samples used for growth rate measurement. The bacterial strains were exposed to the nanoparticles in the dark for six hours at 37°C. Following incubation, 1 mL of the culture was transferred to a sterile agar plate and incubated for 24 h under the same conditions as the liquid cultures. All samples were prepared in duplicate and cultures without nanoparticles were cultivated in growth media as controls.

2.7. Bacterial Cell Morphology. Cell morphology of *E. coli* and *S. aureus* was determined using the same unmodified and APTS-, PEG-, and TEOS-modified magnetite (1 g/L) bacterial samples used for determination of growth rate. Cells with nanoparticles (1 g/L) were stained using 4′,6-diamidino-2-phenylindole (DAPI) and observed under an AxioImager fluorescence microscope (Zeiss, Germany) at 365/461 nm excitation/emission. Length of *E. coli* cells was measured for samples with nanoparticles (incubated for six hours) and for a control without nanoparticles.

2.8. Statistical Analysis. All results were analysed using ANOVA (GraphPad Prism software; CA, USA). Dunnett's multicomparison test was used to compare differences between the means of *E. coli* and *S. aureus* growth rate, while values for CFU and bacterial cell length were compared using Sidak's multicomparison test.

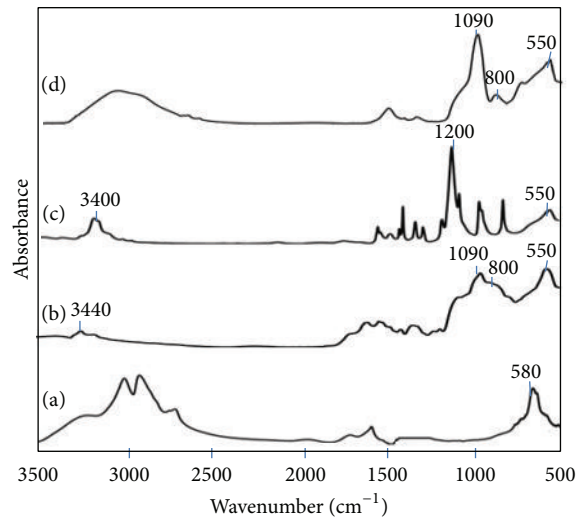

Figure 1: Infrared spectroscopic scans of (a) unmodified magnetite nanoparticles, (b) APTS-magnetite, (c) PEG-magnetite, and (d) TEOS-magnetite.

3. Results and Discussion

3.1. Characterization of Magnetic Nanoparticles. In each case, functional groups on the surface of the magnetite nanoparticles were detected by IR (Figure 1), with absorption peak at 580 cm^{-1} confirming the presence of an Fe–O bond related to the magnetite phase of magnetite nanoparticles [42]. Bands at 800 cm^{-1} and 1090 cm^{-1} were due to symmetric and asymmetric linear vibrations of Si–O–Si, indicative of formation of a silica shell with APTS- and TEOS-modified magnetite. The absorption contribution from the free $-NH_2$ group of APTS-modified magnetite appeared at 3440 cm^{-1}. Absorption bands at 3400 cm^{-1} and 1200 cm^{-1} were assignable to O–H stretching and C–O of PEG-modified magnetite.

DLS indicated that unmodified magnetite nanoparticles display a wider size range than modified magnetite nanoparticles. Presence of an APTS, PEG, or TEOS layer on the nanoparticle surface increased average particle size (Figure 2), with an average increase of 89 nm for unmodified nanoparticles and 123 nm, 109 nm, and 130 nm for APTS-, PEG-, and TEOS-modified magnetite nanoparticles, respectively.

The zeta potential for unmodified magnetite nanoparticles was 36.9 mV and 12.2 mV, 23.1 mV, and 36.2 mV for APTS-, PEG-, and TEOS-modified magnetite nanoparticles, respectively. The nanoparticle's zeta potential (surface charge) indicates how effectively nanoparticles form stable or aggregated colloids during the colloidal phase. At low zeta potentials (close to zero), particles are no longer repelled strongly and colloids will aggregate due to attractive surface forces. Conversely, stable dispersions are formed at high zeta

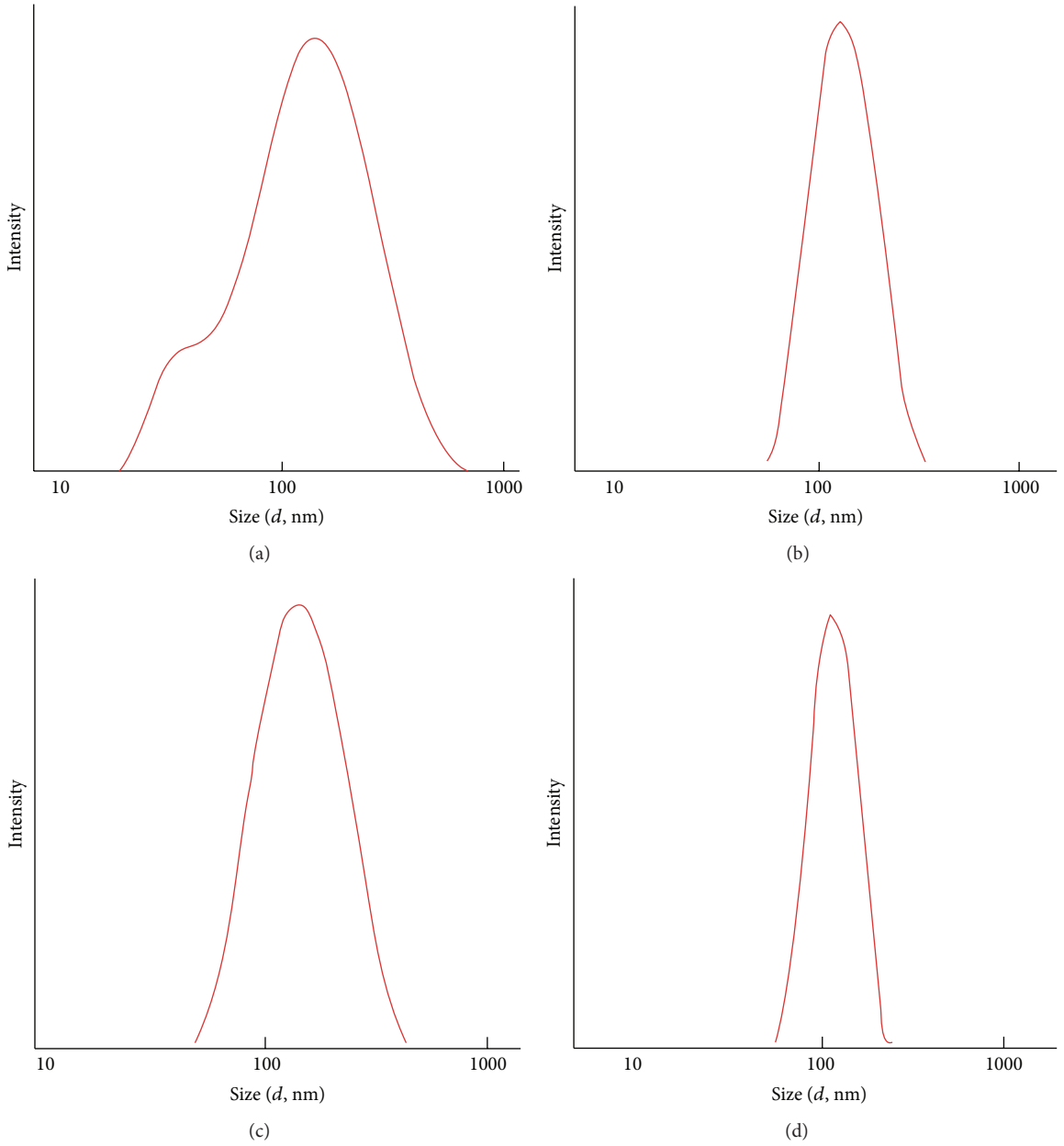

Figure 2: Hydrodynamic diameters of (a) unmodified magnetite nanoparticles, (b) APTS-magnetite, (c) PEG-magnetite, and (d) TEOS-magnetite.

potentials (above ~30 mV). This is of particular importance in water treatment and biomedicine applications where stable colloidal systems are required.

SEM indicated slight differences in the morphology of unmodified and modified magnetite nanoparticles (Figure 3). Unlike modified magnetite nanoparticles, unmodified nanoparticles, which showed a broader size distribution, were usually agglomerated due to the high surface energy between the nanoparticles and dipole-dipole interactions. In addition, we detected a higher number of modified magnetite nanoparticles, providing further evidence for insertion of a surface layer on the magnetite.

3.2. Effect of Surface-Modified Magnetite on Bacteria. The growth rates of Gram-negative *E. coli* and Gram-positive *S. aureus* control solutions (nutrient broth without nanoparticles) were 0.24 and 0.18 doublings/h, respectively. Unmodified magnetite nanoparticles had no significant effect on the growth rate of either bacteria. Interestingly, however, the growth rates of both bacteria were negatively correlated with suspension concentration (0.05, 0.3, 0.6, and 1 g/L) in APTS-, PEG-, and TEOS-modified nanoparticle solutions (Figure 4).

E. coli growth rate dropped to 0.15 doublings/h when incubated with APTS-magnetite (1 g/L), while growth rates for PEG- and TEOS-magnetite (1 g/L) were 0.22 and

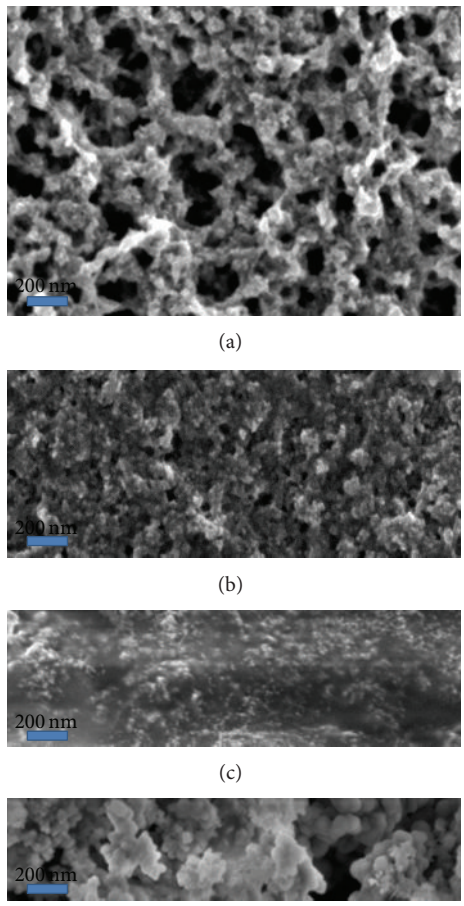

Figure 3: Scanning electron microscope images of (a) unmodified magnetite nanoparticles, (b) APTS-magnetite, (c) PEG-magnetite, and (d) TEOS-magnetite. Scale bar = 200 nm.

0.18 doublings/h, respectively. At all concentrations, APTS-magnetite had a greater effect on *E. coli* growth rate than the other modified magnetite nanoparticles (Figure 4). Growth rates of *S. aureus* exposed to APTS-, PEG-, and TEOS-magnetite were 0.09, 0.13, and 0.1 doublings/h, respectively (Figure 4).

The EC10 for growth inhibition on both *E. coli* and *S. aureus* in unmodified and modified nanoparticle solutions indicated that modified nanoparticles had a greater effect on *S. aureus* than *E. coli*, with PEG-magnetite nanoparticles having the least effect on growth rate of either bacteria (Table 1). Both APTS-magnetite and TEOS-magnetite (1 g/L) had a significant negative effect (ANOVA; $P < 0.0001$) on both *E. coli* and *S. aureus* growth.

The effect of modified magnetite on bacterial growth rate was further supported by results obtained from the colony-forming assay. Compared to control samples with no nanoparticles, *E. coli* CFU declined to 73% with APTS-magnetite and 63.6% with TEOS-magnetite, whilst that for *S. aureus* declined to 27% with APTS-magnetite and 38% with TEOS-magnetite, after six hours of exposure (Figure 5). This confirms a similar effect determined for growth rate in both

Table 1: The effective concentration at 10% inhibition, EC10 (g/L) of unmodified and modified magnetite nanoparticles determined for Gram-negative *Escherichia coli* and Gram-positive *Staphylococcus aureus*.

	Unmodified magnetite	APTS-magnetite	PEG-magnetite	TEOS-magnetite
E. coli	0.60	0.170	0.509	0.325
S. aureus	NOEC < 1	0.108	0.259	0.128

bacterial strains. Comparison of viable cells using ANOVA indicated that APTS-magnetite had a greater impact on *S. aureus* ($P = 0.0019$) than TEOS-magnetite ($P = 0.0086$). On the other hand, both APTS- and TEOS-magnetite had no significant effect on *E. coli* ($P = 0.2$ and $P = 0.13$).

In order to elucidate these results further, we compared bacterial cell morphology using fluorescence microscopy after DAPI staining. Notably, *E. coli* showed rapid cell elongation ($3.8 \pm 0.12\,\mu$m to $6.5 \pm 0.5\,\mu$m after six hours; $P = 0.0001$) when exposed to APTS-magnetite in soya broth media (Figure 6). Moreover, *E. coli* cells were clearly attached to the APTS-magnetite particles while the grape-like clusters of *S. aureus* were irregularly grouped with more single cells than cell clusters.

3.3. Factors Affecting Biological Stress. Our results indicate that APTS-, TEOS-, and PEG-magnetite nanoparticles had a significantly greater biological effect on *S. aureus* than on *E. coli*. Many variables may impact on biological effect, including both biological (e.g., bacterial cell structure, cell growth rate, biofilm formation, stress/toxicity mechanisms) and chemical parameters (e.g., pH, ORP). Bacterial cell walls (peptidoglycan layers) are designed to protect the intracellular matrix while allowing for nutrient transport. In doing so they help to maintain the structural strength of the cell and stabilize the osmotic pressure of the cytoplasm and they are involved in binary fission during bacterial cell reproduction [43, 44]. Gram-positive cells possess a thick peptidoglycan layer of 20–50 nm [45], while Gram-negative cells contain a thin peptidoglycan layer. Notably, in our study, *E. coli* cells in contact with APTS-magnetite were unable to divide as the cells had increased in length from $3.8\,\mu$m to $6.5\,\mu$m. Further, Gram-negative cell walls comprise an outer membrane, which covers the surface membrane and is often resistant to compounds such as detergents, and a lipopolysaccharide layer, which is essential for cell viability and contributes to the negative charge of the membrane [46]. An increased negative surface charge could reduce the likelihood of *E. coli* interacting with nanoparticles, as reflected in the lowered effect on Gram-positive *S. aureus* in this study.

Bacterial growth rate is a good method for indicating tolerance of bacteria to nanoparticles. Fast-growing bacteria, for example, are more susceptible to antibiotics and nanoparticles than slow-growing bacteria [47, 48]. The hindered growth observed in *E. coli* and *S. aureus* in this study could be related to expression of stress-response genes [49, 50]. Gram-positive bacteria have the ability to form a biofilm to protect

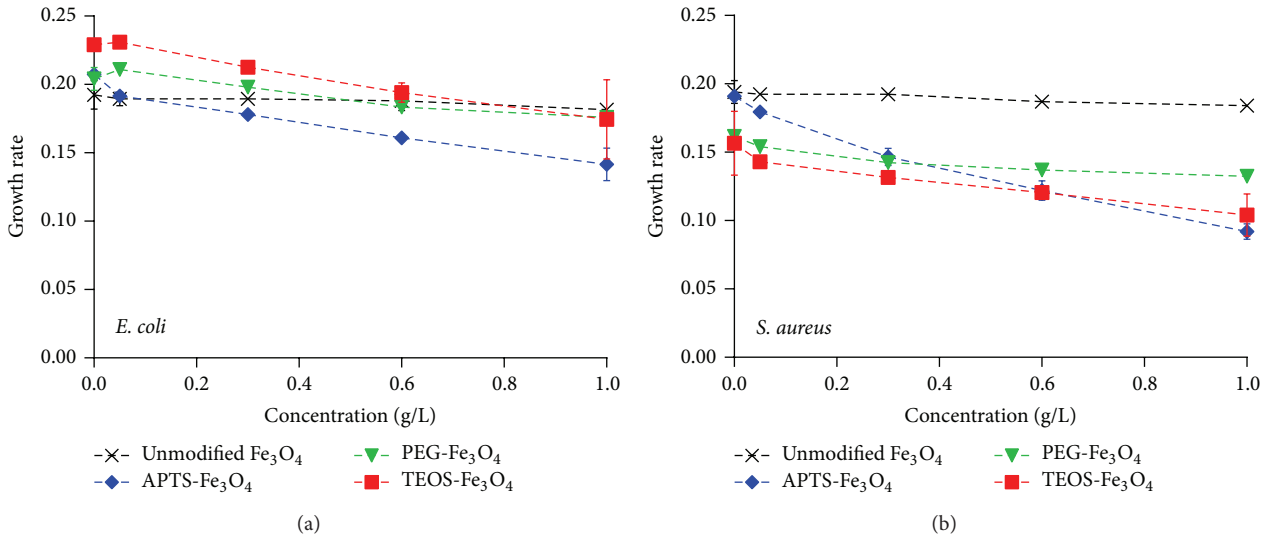

Figure 4: Growth rate (doublings/h) of *Escherichia coli* (a) and *Staphylococcus aureus* (b) after six hours of incubation with unmodified and modified APTS-, PEG-, and TEOS-magnetite. The error bars were determined from $n = 2$.

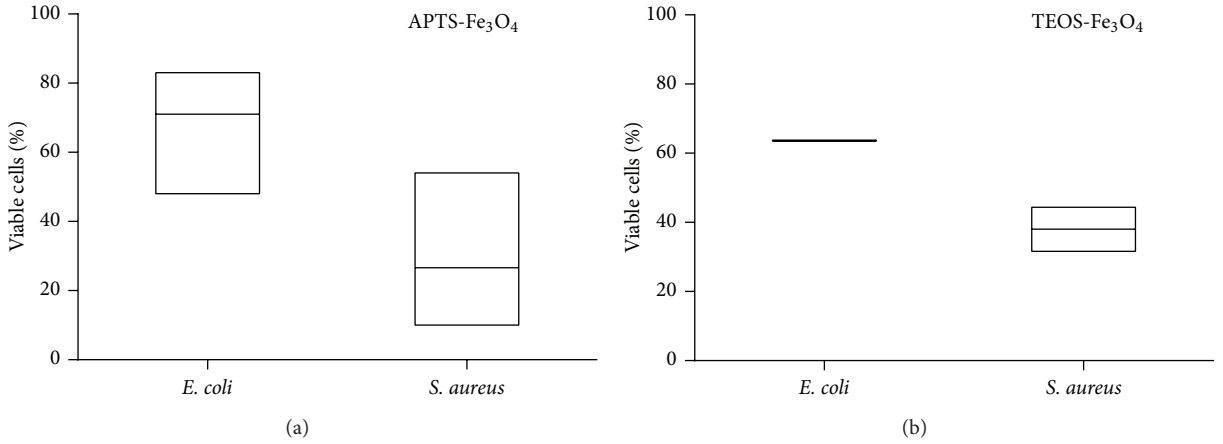

Figure 5: Proportion of viable cells (colony forming units) after six hours of exposure to 1 g/L APTS-magnetite (a) and 1 g/L TEOS-magnetite (b) comparing to control (without nanoparticles) = 100%.

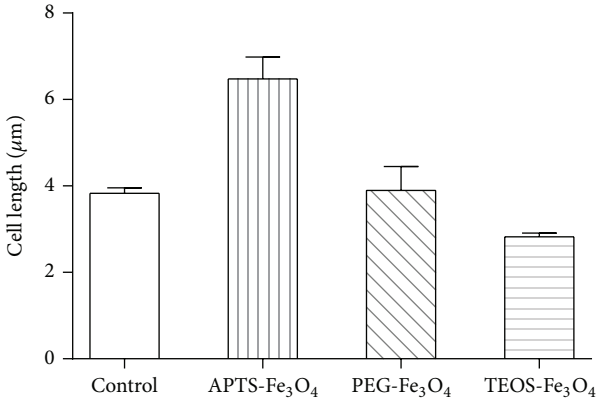

Figure 6: Length of *Escherichia coli* cells after six hours of exposure to surface-modified magnetite nanoparticles. The error bars show standard error of the mean.

themselves under stressful conditions (*Pseudomonas* sp., e.g., develop a biofilm in the presence of heavy metals) [51]. In our study, Gram-positive *S. aureus* aggregated into large grape-like clusters after six hours of incubation with unmodified and APTS-, TEOS-, and PEG-modified magnetite. Previous studies have also reported that magnetite nanoparticles have a considerable capacity to penetrate biofilms [52, 53]. By interacting with the outer membrane, nanoparticles may cause loss of membrane integrity in bacteria and change the cell's structure. Such damage could lead to an increase in membrane permeability and leakage of intracellular constituents [54–56] and, indirectly, generate reactive oxidation species (ROS) through the Fenton reaction [57]. Zero-valent iron, for example, causes cell membrane disruption in *E. coli* [54] and adsorption on cells and ROS generation in *Bacillus subtilis* var. *niger* and *Pseudomonas fluorescens* [58]. In this study, magnetite nanoparticles are likely to have created

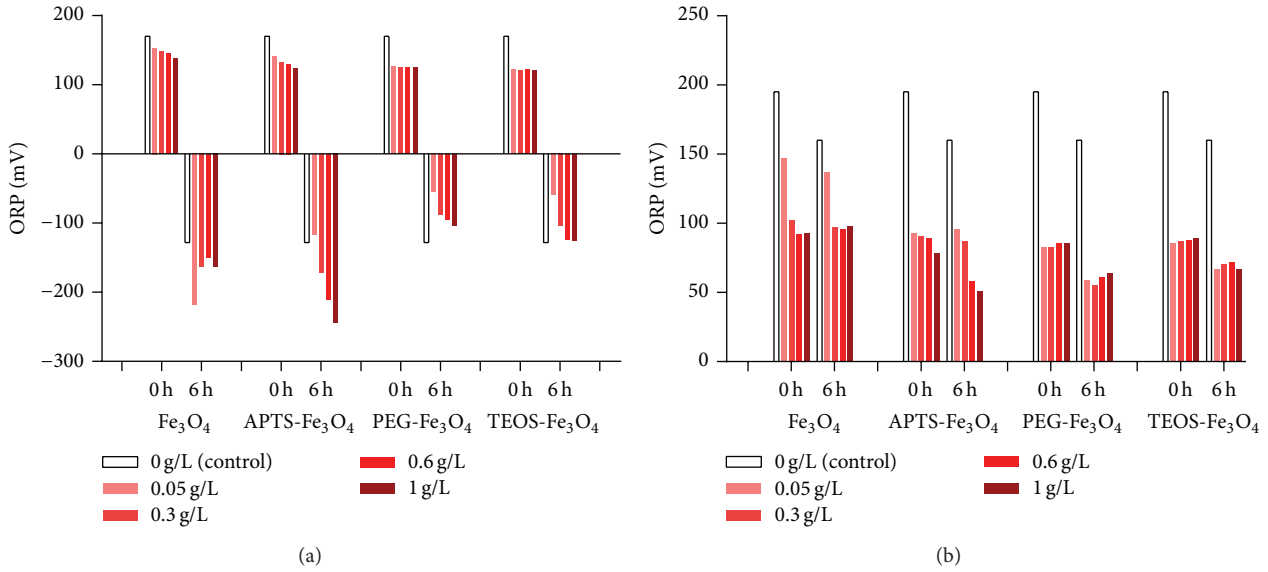

FIGURE 7: Oxidation/reduction potential (ORP) of (a) *Escherichia coli* and (b) *Staphylococcus aureus* cultures at time zero and after six hours of incubation with modified magnetite nanoparticles.

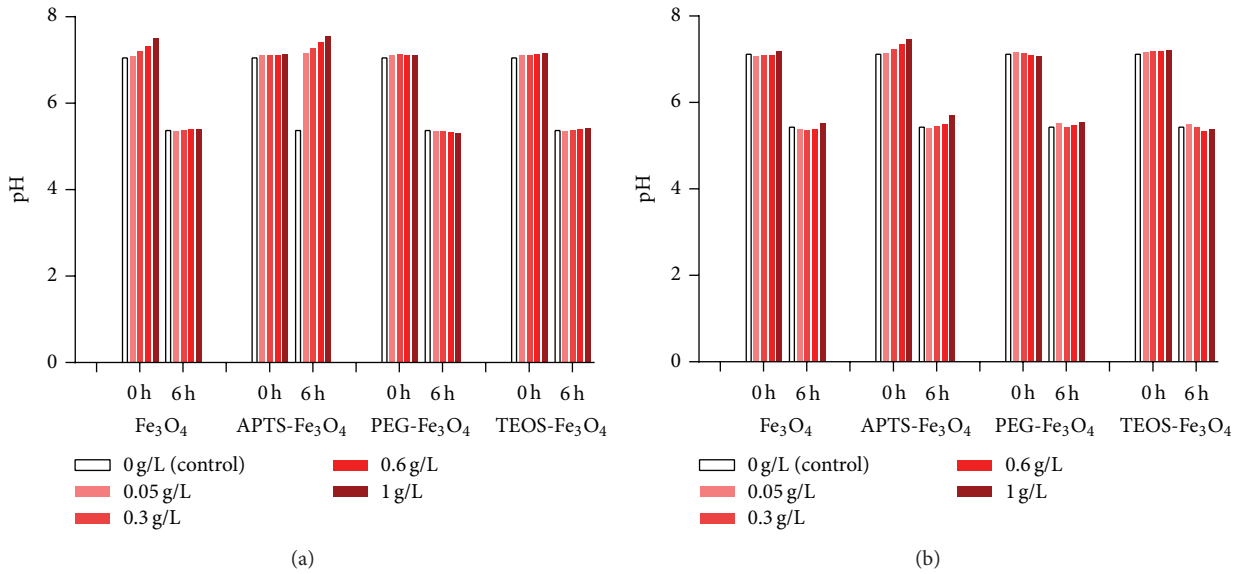

FIGURE 8: pH values for *Escherichia coli* (a) and *Staphylococcus aureus* (b) cultures at time zero and after six hours of incubation with modified magnetite nanoparticles.

stressful conditions via ROS generation, which significantly inhibited *S. aureus* growth. Additionally, pH values obtained in parallel with bacterial growth experiments at the start and end of the experiment were similar to those of the controls (*E. coli* or *S. aureus* culture alone), with initial pH being neutral and dropping to around pH 5 after six hours, with or without the presence of magnetic nanoparticles (Figure 7). Only in the case of *E. coli* cultured with APTS-magnetite did the neutral pH remain unchanged after six hours, remaining within the optimum pH range of 6-7 for *E. coli* growth [59]. Furthermore, the negative ORP of *E. coli* and positive ORP of *S. aureus* both showed similar trends in both treated and untreated cultures (Figure 8). In our biological effect tests, therefore, pH and ORP could not be considered as indicators for stressed bacterial states (Figures 7 and 8).

In summary, magnetite nanoparticles surface-functionalized with APTS and TEOS had a significant biological effect on Gram-positive *S. aureus*, while PEG-nanoparticles did not. In contrast, none of the functionalized magnetite nanoparticles showed any statistically significant effect on Gram-negative *E. coli*.

4. Conclusion

Functionalized modified magnetite nanoparticles (TEOS-, PEG-, and APTS-magnetite) were prepared using coprecipitation and characterized with SEM and IR. Testing for

biological effect indicated that PEG-magnetite can be considered as safe nontoxic material. TEOS-magnetite showed stronger effect only towards *S. aureus*. APTS-magnetite nanoparticles display a degree of antimicrobial activity, allowing for their use in bioapplications such as drug nanocarriers, where bacterial growth is undesirable.

Conflict of Interests

The authors declare that there is no conflict of interests regarding the publication of this paper.

Acknowledgments

The results of this project (LO1201) were obtained through the financial support of the Ministry of Education, Youth and Sports under the framework of targeted support from the "National Programme for Sustainability I", the OPR&DI project Centre for Nanomaterials, Advanced Technologies and Innovation (CZ.1.05/2.1.00/01.0005), and "Project Development for Research Teams of R&D Projects" at the Technical university of Liberec (CZ.1.07/2.3.00/30.0024).

References

[1] S. Mondini, S. Cenedese, G. Marinoni et al., "One-step synthesis and functionalization of hydroxyl-decorated magnetite nanoparticles," *Journal of Colloid and Interface Science*, vol. 322, no. 1, pp. 173–179, 2008.

[2] K. G. Paul, T. B. Frigo, J. Y. Groman, and E. V. Groman, "Synthesis of ultrasmall superparamagnetic iron oxides using reduced polysaccharides," *Bioconjugate Chemistry*, vol. 15, no. 2, pp. 394–401, 2004.

[3] J. Namanga, J. Foba, D. T. Ndinteh, D. M. Yufanyi, and R. W. M. Krause, "Synthesis and magnetic properties of a superparamagnetic nanocomposite 'pectin-magnetite nanocomposite'," *Journal of Nanomaterials*, vol. 2013, Article ID 137275, 8 pages, 2013.

[4] C. C. Gonzalez, C. A. M. Pérez, A. M. Martínez et al., "Development of antibody-coated magnetite nanoparticles for biomarker immobilization," *Journal of Nanomaterials*, vol. 2014, Article ID 978284, 7 pages, 2014.

[5] X. Cao, B. Zhang, F. Zhao, and L. Feng, "Synthesis and properties of MPEG-coated superparamagnetic magnetite nanoparticles," *Journal of Nanomaterials*, vol. 2012, Article ID 607296, 6 pages, 2012.

[6] D. K. Yi, S. S. Lee, and J. Y. Ying, "Synthesis and applications of magnetic nanocomposite catalysts," *Chemistry of Materials*, vol. 18, no. 10, pp. 2459–2461, 2006.

[7] D. K. Yi, S. S. Lee, G. C. Papaefthymiou, and J. Y. Ying, "Nanoparticle architectures templated by SiO_2/Fe_2O_3 nanocomposites," *Chemistry of Materials*, vol. 18, no. 3, pp. 614–619, 2006.

[8] D. C. Lee, F. V. Mikulec, J. M. Pelaez, B. Koo, and B. A. Korgel, "Synthesis and magnetic properties of silica-coated FePt nanocrystals," *Journal of Physical Chemistry B*, vol. 110, no. 23, pp. 11160–11166, 2006.

[9] C. R. Vestal and Z. J. Zhang, "Synthesis and magnetic characterization of mn and Co spinel ferrite-silica nanoparticles with tunable magnetic core," *Nano Letters*, vol. 3, no. 12, pp. 1739–1743, 2003.

[10] T.-J. Yoon, K. N. Yu, E. Kim et al., "Specific targeting, cell sorting, and bioimaging with smart magnetic silica core-shell nanomaterials," *Small*, vol. 2, no. 2, pp. 209–215, 2006.

[11] S. M. Moghimi, A. C. Hunter, and J. C. Murray, "Long-circulating and target-specific nanoparticles: theory to practice," *Pharmacological Reviews*, vol. 53, no. 2, pp. 283–318, 2001.

[12] W. Wu, Q. He, and C. Jiang, "Magnetic iron oxide nanoparticles: synthesis and surface functionalization strategies," *Nanoscale Research Letters*, vol. 3, no. 11, pp. 397–415, 2008.

[13] H. Xuemei and Y. Hao, "Fabrication of polystyrene/detonation nanographite composite microspheres with the core/shell structure via pickering emulsion polymerization," *Journal of Nanomaterials*, vol. 2013, Article ID 751497, 8 pages, 2013.

[14] R. T. Yang, *Adsorbents: Fundamentals and Applications*, John Wiley & Sons, 2003.

[15] W. Zhao, J. Gu, L. Zhang, H. Chen, and J. Shi, "Fabrication of uniform magnetic nanocomposite spheres with a magnetic core/mesoporous silica shell structure," *Journal of the American Chemical Society*, vol. 127, no. 25, pp. 8916–8917, 2005.

[16] S. D. Steichen, M. Caldorera-Moore, and N. A. Peppas, "A review of current nanoparticle and targeting moieties for the delivery of cancer therapeutics," *European Journal of Pharmaceutical Sciences*, vol. 48, no. 3, pp. 416–427, 2013.

[17] D. D. Herea and H. Chiriac, "One-step preparation and surface activation of magnetic iron oxide nanoparticles for bio-medical applications," *Optoelectronics and Advanced Materials—Rapid Communications*, vol. 2, no. 9, pp. 549–552, 2008.

[18] J. Wang, S. Zheng, Y. Shao, J. Liu, Z. Xu, and D. Zhu, "Amino-functionalized Fe_3O_4@SiO_2 core-shell magnetic nanomaterial as a novel adsorbent for aqueous heavy metals removal," *Journal of Colloid and Interface Science*, vol. 349, no. 1, pp. 293–299, 2010.

[19] H. Hu, Z. Wang, and L. Pan, "Synthesis of monodisperse Fe_3O_4@silica core-shell microspheres and their application for removal of heavy metal ions from water," *Journal of Alloys and Compounds*, vol. 492, no. 1-2, pp. 656–661, 2010.

[20] A. K. Gupta and S. Wells, "Surface-modified superparamagnetic nanoparticles for drug delivery: preparation, characterization, and cytotoxicity studies," *IEEE Transactions on Nanobioscience*, vol. 3, no. 1, pp. 66–73, 2004.

[21] M. S. A. Darwish, U. Peuker, U. Kunz, and T. Turek, "Bi-layered polymer-magnetite core/shell particles: synthesis and characterization," *Journal of Materials Science*, vol. 46, no. 7, pp. 2123–2134, 2011.

[22] M. S. A. Darwish, U. Kunz, and U. Peuker, "Preparation and catalytic use of platinum in magnetic core/shell nanocomposites," *Journal of Applied Polymer Science*, vol. 129, no. 4, pp. 1806–1811, 2013.

[23] W. Stöber, A. Fink, and E. Bohn, "Controlled growth of monodisperse silica spheres in the micron size range," *Journal of Colloid And Interface Science*, vol. 26, no. 1, pp. 62–69, 1968.

[24] Y. Lu, Y. Yin, B. T. Mayers, and Y. Xia, "Modifying the surface properties of superparamagnetic iron oxide nanoparticles through a sol-gel approach," *Nano Letters*, vol. 2, no. 3, pp. 183–186, 2002.

[25] M. Mahmoudi, M. A. Shokrgozar, S. Sardari et al., "Irreversible changes in protein conformation due to interaction with superparamagnetic iron oxide nanoparticles," *Nanoscale*, vol. 3, no. 3, pp. 1127–1138, 2011.

[26] J. Raheb, M. E. Kafayati, M. T. Angazi, S. Alizadeh, and H. Bardania, "The effect of magnetic Fe_3O_4 nanoparticles on the growth of genetically manipulated bacterium, Pseudomonas

aeruginosa (PTSOX4)," *Iranian Journal of Biotechnology*, vol. 11, no. 1, pp. 41–46, 2013.

[27] E. N. Taylor and T. J. Webster, "The use of superparamagnetic nanoparticles for prosthetic biofilm prevention," *International journal of nanomedicine*, vol. 4, pp. 145–152, 2009.

[28] N. Tran, A. Mir, D. Mallik, A. Sinha, S. Nayar, and T. J. Webster, "Bactericidal effect of iron oxide nanoparticles on *Staphylococcus aureus*," *International Journal of Nanomedicine*, vol. 5, no. 1, pp. 277–283, 2010.

[29] M. Senthil and C. Ramesh, "Biogenic synthesis of Fe_3O_4 nanoparticles using tridax procumbens leaf extract and its antibacterial activity on Pseudomonas aeruginosa," *Digest Journal of Nanomaterials and Biostructures*, vol. 7, no. 4, pp. 1655–1661, 2012.

[30] S. S. Behera, J. K. Patra, K. Pramanik, N. Panda, and H. Thatoi, "Characterization and evaluation of antibacterial activities of chemically synthesized iron oxide nanoparticles," *World Journal of Nano Science and Engineering*, vol. 2, pp. 196–200, 2012.

[31] S. L. Iconaru, A. M. Prodan, P. Le Coustumer, and D. Predoi, "Synthesis and antibacterial and antibiofilm activity of iron oxide glycerol nanoparticles obtained by coprecipitation method," *Journal of Chemistry*, vol. 2013, Article ID 412079, 6 pages, 2013.

[32] B. Stephen Inbaraj, T.-Y. Tsai, and B.-H. Chen, "Synthesis, characterization and antibacterial activity of superparamagnetic nanoparticles modified with glycol chitosan," *Science and Technology of Advanced Materials*, vol. 13, no. 1, Article ID 015002, 2012.

[33] D. E. Mihaiescu, M. Horja, I. Gheorghe et al., "Water soluble magnetite nanoparticles for antimicrobial drugs delivery," *Letters in Applied NanoBioScience*, vol. 1, pp. 45–49, 2012.

[34] M. Ming, Y. Zhang, W. Yu, H.-Y. Shen, H.-Q. Zhang, and N. Gu, "Preparation and characterization of magnetite nanoparticles coated by amino silane," *Colloids and Surfaces A: Physicochemical and Engineering Aspects*, vol. 212, no. 2-3, pp. 219–226, 2003.

[35] A. M. Demin, M. A. Uimin, N. N. Shchegoleva, A. E. Yermakov, and V. P. Krasnov, "Surface modification of Fe_3O_4 magnetic nanoparticles with (S)-naproxen," *Nanotechnologies in Russia*, vol. 7, no. 3-4, pp. 132–139, 2012.

[36] S. A. Jayanthi, D. Sukanya, A. J. Pragasam, and P. Sagayaraj, "The influence of PEG 20,000 concentration on the size control and magnetic properties of functionalized bio-compatible magnetic nanoparticles," *Der Pharma Chemica*, vol. 5, pp. 90–102, 2013.

[37] J. Sun, S. Zhou, P. Hou et al., "Synthesis and characterization of biocompatible Fe_3O_4 nanoparticles," *Journal of Biomedical Materials Research Part A*, vol. 80, no. 2, pp. 333–341, 2007.

[38] S. C. Pang, S. Y. Kho, and S. F. Chin, "Fabrication of magnetite/silica/Titania core-shell nanoparticles," *Journal of Nanomaterials*, vol. 2012, Article ID 427310, 6 pages, 2012.

[39] H.-S. Yang, S.-Y. Choi, S.-H. Hyun, H.-H. Park, and J.-K. Hong, "Ambient-dried low dielectric SiO_2 aerogel thin film," *Journal of Non-Crystalline Solids*, vol. 221, no. 2-3, pp. 151–156, 1997.

[40] M. Mahdavi, M. B. Ahmad, M. J. Haron, Y. Gharayebi, K. Shameli, and B. Nadi, "Fabrication and characterization of SiO_2/(3-aminopropyl)triethoxysilane-coated magnetite nanoparticles for lead(II) removal from aqueous solution," *Journal of Inorganic and Organometallic Polymers and Materials*, vol. 23, no. 3, pp. 599–607, 2013.

[41] K. D. Kim, S. S. Kim, Y. Choa, and H. T. Kim, "Formation and surface modification of Fe_3O_4 nanoparticles by co-precipitation and sol-gel method," *J. Ind. Eng. Chem*, vol. 13, no. 7, pp. 1137–1141, 2007.

[42] P. E. García Casillas, C. A. Rodriguez Gonzalez, and C. A. Martínez Pérez, *Infrared Spectroscopy of Functionalized Magnetic Nanoparticles, Infrared Spectroscopy—Materials Science, Engineering and Technology*, edited by T. Theophile, 2012.

[43] J. R. Scott and T. C. Barnett, "Surface proteins of gram-positive bacteria and how they get there," *Annual Review of Microbiology*, vol. 60, pp. 397–423, 2006.

[44] F. Van den Ent, L. A. Amos, and J. Löwe, "Prokaryotic origin of the actin cytoskeleton," *Nature*, vol. 413, no. 6851, pp. 39–44, 2001.

[45] F. van den Ent, C. M. Johnson, L. Persons, P. de Boer, and J. Löwe, "Bacterial actin MreB assembles in complex with cell shape protein RodZ," *The EMBO Journal*, vol. 29, no. 6, pp. 1081–1090, 2010.

[46] I. S. Roberts, "The biochemistry and genetics of capsular polysaccharide production in bacteria," *Annual Review of Microbiology*, vol. 50, pp. 285–315, 1996.

[47] M. R. W. Brown, D. G. Allison, and P. Gilbert, "Resistance of bacterial biofilms to antibiotics: a growth-rate related effect?" *Journal of Antimicrobial Chemotherapy*, vol. 22, no. 6, pp. 777–780, 1988.

[48] T.-F. C. Mah and G. A. O'Toole, "Mechanisms of biofilm resistance to antimicrobial agents," *Trends in Microbiology*, vol. 9, no. 1, pp. 34–39, 2001.

[49] C. Lu, M. J. Brauer, and D. Botstein, "Slow growth induces heat-shock resistance in normal and respiratory-deficient yeast," *Molecular Biology of the Cell*, vol. 20, no. 3, pp. 891–903, 2009.

[50] P. S. Stewart, "Mechanisms of antibiotic resistance in bacterial biofilms," *International Journal of Medical Microbiology*, vol. 292, no. 2, pp. 107–113, 2002.

[51] C.-C. Chien, B.-C. Lin, and C.-H. Wu, "Biofilm formation and heavy metal resistance by an environmental *Pseudomonas* sp," *Biochemical Engineering Journal*, vol. 78, pp. 132–137, 2013.

[52] M. Mahmoudi and V. Serpooshan, "Silver-coated engineered magnetic nanoparticles are promising for the success in the fight against antibacterial resistance threat," *ACS Nano*, vol. 6, no. 3, pp. 2656–2664, 2012.

[53] H. Park, H.-J. Park, J. A. Kim et al., "Inactivation of *Pseudomonas aeruginosa* PA01 biofilms by hyperthermia using superparamagnetic nanoparticles," *Journal of Microbiological Methods*, vol. 84, no. 1, pp. 41–45, 2011.

[54] M. Auffan, W. Achouak, J. Rose et al., "Relation between the redox state of iron-based nanoparticles and their cytotoxicity toward *Escherichia coli*," *Environmental Science & Technology*, vol. 42, no. 17, pp. 6730–6735, 2008.

[55] D. B. Zorov, C. R. Filburn, L. O. Klotz, J. L. Zweier, and S. J. Sollott, "Reactive oxygen species (ROS)-induced ROS release: a new phenomenon accompanying induction of the mitochondrial permeability transition in cardiac myocytes," *The Journal of Experimental Medicine*, vol. 192, no. 7, pp. 1001–1014, 2000.

[56] D. B. Zorov, M. Juhaszova, and S. J. Sollott, "Mitochondrial ROS-induced ROS release: an update and review," *Biochimica et Biophysica Acta*, vol. 1757, no. 5-6, pp. 509–517, 2006.

[57] A. Ševců, Y. S. El-Temsah, E. J. Joner, and M. Černík, "Oxidative stress induced in microorganisms by zero-valent iron nanoparticles," *Microbes and Environments*, vol. 26, no. 4, pp. 271–281, 2011.

[58] M. Diao and M. Yao, "Use of zero-valent iron nanoparticles in inactivating microbes," *Water Research*, vol. 43, no. 20, pp. 5243–5251, 2009.

[59] P. M. Desmarchelier and N. Fegan, "Enteropathogenic *Escherichia coli*," in *Foodborne Microorganisms of Public Health Significance*, A. D. Hocking, Ed., chapter 9, pp. 267–310, Australian Institute of Food Science and Technology (NSW Branch), Sydney, Australia, 6th edition, 2003.